RSC Advances

ROYAL SOCIETY OF CHEMISTRY

www.rsc.org/advances

Low-temperature synthesis of Cu_2CoSnS_4 nanoparticles by thermal decomposition of metal precursors and study of its structural, optical and electrical properties for photovoltaic application

Mokurala Krishnaiah*, Parag Bhargava, and Sudhanshu Mallick

Department of Metallurgical Engineering & Materials Science, Indian Institute of Technology Bombay, Mumbai-400076

Email address:krishna887@iitb.ac.in, Telephone number: +912225767641, Fax: +912225726975

Abstract: Copper-based chalcogenide quaternary semiconductor Cu_2CoSnS_4 (CCTS) have emerged as a promising material for thin film photovoltaic devices due to its opto-electrical properties, and earth-abundant composition. The present study reports the synthesis of CCTS nanoparticles by a robust, solvent free, single step thermal decomposition process and their application in photovoltaics. Detailed studies of the effect of synthesis parameters (temperature, time) on crystallization, the elemental composition of CCTS nanoparticles are reported. Physical, optical and electrical characterization of as-synthesized nanoparticles and sulfurized films were carried out. The morphology and elemental composition of synthesized nanoparticles are found to be similar to the nanoparticles synthesized by conventional solution processes. Electrical properties of CCTS films are reported for first time and are found to be the carrier mobility (μ) = 36 cm^2/Vs, carrier concentration (n) = $2x10^{16}$ cm^{-3}, resistivity = $3x10^{-3}$ Ωm. Mott-Schottky analysis confirmed the p-type conductivity of the CCTS film. The films fabricated from the as-synthesized nanoparticles showed a photoresponse under illumination (100 mW/cm^2). The optimum optical band gap (1.46 eV) and photoresponse of the CCTS film indicate that it can act as a promising cost-effective absorber layer for thin film solar cells.

Keywords: Inorganic semiconductors; quaternary chalcopyrite nanomaterials; thermal decomposition process; optical and electrical properties.

1. Introduction

Copper-based quaternary chalcopyrite nanomaterials are the most promising absorbing materials in thin-film photovoltaics (PV) devices due to their unique structural and electrical properties [1]. Conventionally, these sulfide-based thin-film solar cells have been fabricated using vacuum based techniques and showed an efficiency of 21.7% for Cu (In, Ga)(Se, $S)_2$ (CIGSSe) solar cells [2]. However, the fabrication cost and scarcity of the constituent elements (In, Ga) increase the overall cost of the PV devices. Usage of earth abundant quaternary chalcopyrites (Cu_2ZnSn (S, $Se)_4$ (CZTSSe), Cu_2FeSnS_4 (CFTS), Cu_2NiSnS_4 (CNTS), Cu_2CoSnS_4 (CCTS)), and solution based processes are alternative ways to make the thin-film solar cells economically viable [1]. Till date, a cell efficiency of 12.5 % and 9.2 % has been reported for CIGSSe and CZTSSe respectively using a nanocrystalline ink-based process [3 - 5]. An efficiency of 15.2 % and 12.7 % for CIGSSe and CZTSSe based PV devices respectively were reported by spin coating of hydrazine solution based process [3, 6]. On the other hand, CCTS nanoparticles are still at the stage of material synthesis and characterization only [7 - 12]. Previously, optical, thermoelectric properties and photoelectric response of CCTS nanoparticles had been reported [8 - 12]. However, Phase purity of sulfurized CCTS films and its electrical properties such as resistivity, mobility, carrier concentration and its nature of conductivity have yet not been explored.

Quaternary sulfide nanoparticles have several advantages as compared to metals, binary sulfides, and metal oxide particles presently being used for the preparation of absorber layers [4 - 5]. Nanoparticle ink based absorber layer resulted in a dense film and had uniformity of elemental composition over large areas of the film [4]. Recently, CCTS nanoparticles have been synthesized via solution-based processes such as a high-temperature route [7], hot injection,

solvothermal, and hydrothermal [8 - 12]. However, nanoparticles synthesized via a hot injection method are capped with organic molecules (Oleylamine) and thus limit the performance of optoelectronic devices [13]. Organic molecules act as an insulating barrier between nanoparticles and block the electrical contact between them [12 - 13]. Solvothermal and hydrothermal routes require longer reaction time for the formation of the crystalline phase of the nanomaterials [9, 11]. As an alternative, thermal decomposition of metal precursors is being utilized. As reported in the literature, this simple, single step, inexpensive and low-temperature process, eliminates the usage of hazardous chemicals as well as requires short processing time to get the crystalline CZTS nanoparticles [15].

Here, we report the synthesis of CCTS nanoparticles using single step thermal decomposition of the metal precursors. Synthesized nanoparticles and sulfurized films were characterized for their structural and optical properties. The electrical properties of CCTS films are reported for the first time, and the photoresponse is also analyzed.

2. Experimental details

2.1 Synthesis of CCTS nanoparticles by thermal decomposition of process metal precursors

The detailed synthesis procedure for CCTS nanoparticles was adopted from the authors' previous paper [15]. In brief, the elemental precursor chemicals used for the experimental work were 1.85 mmole $Cu(CH_3COO)_2.H_2O$ (SRL, AR Grade), 1 mmole $CoCl_2.6H_2O$ (Merck, GR grade), 1 mmole $SnCl_2.2H_2O$ (Merck, GR grade) and 12 mmole $CS(NH)_2$ (SD Fine, AR grade). Then, the above precursors were taken in a polypropylene (pp) container along with ethanol and 3 mm diameter zirconia grinding media. This precursor mix was pot milled to get a homogeneous solution, which was then transferred to an alumina crucible that was kept in a tubular furnace. The synthesis process was carried out at a various temperature ranging from

250°C to 450°C for different times (1 - 6 h) in an argon atmosphere. Nanoparticles synthesized at 350°C for 1 h were dispersed in hexanethiol (Sigma-Aldrich) for ink formulation.

2.2 CCTS film deposition by spin coating

Spin coating was used to deposit the CCTS nanoparticle-based ink over fluorine-doped tin oxide (FTO) and soda lime glass (SLG) substrate in a fume hood. The prepared CCTS ink was spin-coated on FTO and SLG substrate at 3000 rpm for 30 s and then dried at 120°C for 3 min on a hot plate. The spin coating and drying processes were repeated several times to obtained the desired thickness. The spin coated films were then sulfurized in the presence of sulfur source in an inert (Ar) atmosphere at 500°C for 30 min.

2.3 Characterization

The crystal structure of synthesized CCTS nanoparticles and sulfurized films were identified by X-ray diffraction (XRD) (PANalytical X-ray diffractometer) and Raman spectroscopy (HORIBA HR800). XRD was performed in the 2θ scan range of 20 – 80 using Cu-K_α irradiation. Raman spectroscopy was performed in the range of 200 – 500 nm using argon excitation with a wavelength of 514.5 nm. The morphology and size of prepared CCTS nanoparticles were examined by field emission gun-transmission electron microscopy (FEG-TEM, JSM7200F). Surface and cross-sectional features of prepared CCTS film were studied using field emission gun-scanning electron microscope (FEG-SEM, JSM-7600F). Elemental composition of the as-synthesized nanoparticles and the sulfurized film was examined using energy dispersive spectrometer (EDS). The optical absorption spectra of CCTS films were collected using a spectrophotometer (LAMBDA UV-750, PerkinElmer) at room temperature within the range of 300 – 900 nm. I-V characteristics of CCTS films, device structure (FTO/CCTS/Au), were studied using an A.M. 1.5 solar simulator (Keithley Instruments, Inc, 100 mW/cm^2) in the

voltage ranging from -10 V to 10 V. The resistivity of films deposited over SLG substrate was measured with the help of four probe technique (Scientific Equipment, India). Electrical properties of the CCTS film coated on the SLG glass substrate were obtained using four probe Hall Effect measurements (Lake Shore, Model 8404 AC/DC) in a dc magnetic field strength of 0.67 T at room temperature. Indium was used for making electrical contact, applied at the corner of square shape CCTS film (7 mm x 7 mm), for Hall measurements. Mott-Schottky (MS) measurement was recorded in an aqueous 0.1 M Na_2SO_4 electrolyte solution using an impedance analyzer (PGSTAT, AUTOLAB 302N). Three electrode electrochemical cell system was used for MS measurements, wherein Ag/AgCl, Pt, and CCTS/FTO/glass were used as a reference electrode, counter electrode and working electrode respectively. The electrolyte pH was adjusted to 9.5 using 1M NaOH solution.

3. Results and discussion

The CCTS nanoparticles are synthesized at various temperatures ranging from 250°C to 450°C for different times (1 - 6 h) to study their effect on the crystallinity of CCTS. We could not see any secondary phases formation at given synthesis conditions. Therefore, in the current manuscript, we are reporting the synthesis of nanoparticles at a temperature range from 250°C to 450°C for 1 h. The XRD patterns of nanoparticles synthesized at different temperatures for 1 h are shown in Fig. 1a. All diffraction peaks present in the Fig.1a correspond to the stannite phase of CCTS (JCPDF No: 260513). The average crystallite size of CCTS nanoparticles is calculated using Debye-Scherer's formula. The crystallite size of nanoparticles synthesized at 250°C, 300°C, 350°C, 400°C, and 450°C for 1 h are found to be 8 nm, 10 nm, 13 nm, 15 nm, and 18 nm respectively. The XRD patterns of CCTS films sulfurized at 500°C for 30 min are shown in Fig. 1b. All diffraction peaks are existing in the Fig. 1b (film coated on SLG substrate) correspond to

the stannite phase of CCTS (JCPDF No: 260513). Other hand, the film coated over FTO substrate (red line: Fig.1b) shows additional peaks (Ψ) corresponding to FTO substrate along with CCTS phase. However, similar XRD patterns of secondary phase like Cu_2SnS_3 and CCTS make the XRD analysis alone to be insufficient for the confirmation of the phase purity of synthesized nanoparticles and sulfurized film.

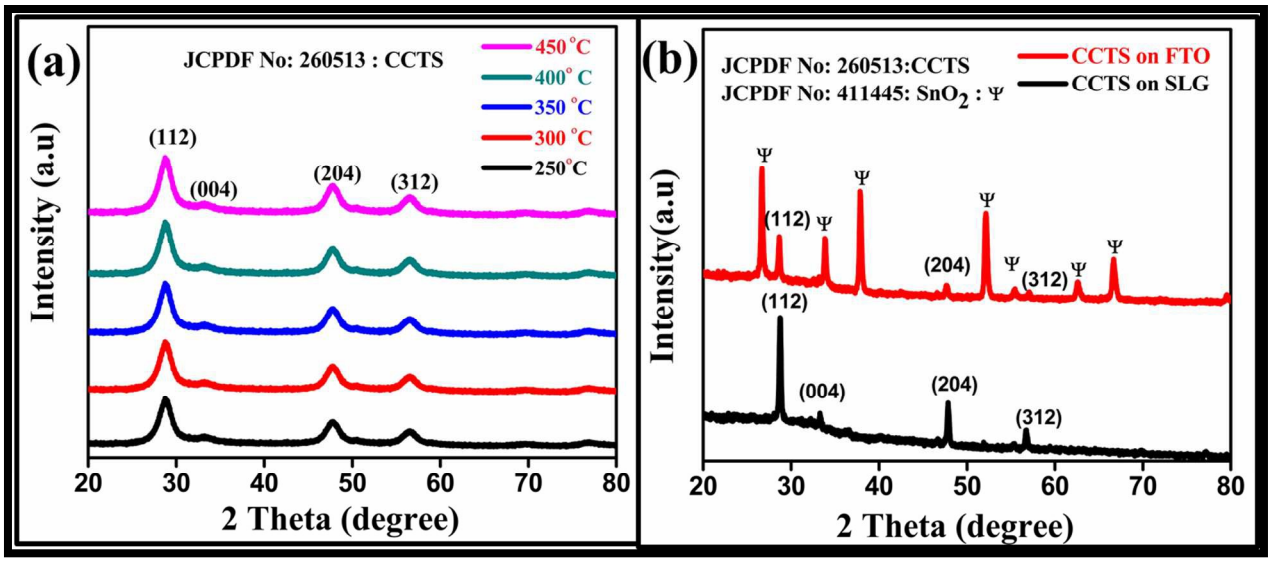

Fig. 1 XRD patterns of CCTS (a) nanoparticles synthesized at 250°C - 450°C for 1h (b) film sulfurized at 500°C for 30 min

Further verification of phase purity of the prepared samples was done using Raman spectroscopy. Raman spectra of the synthesized nanoparticles and sulfurized CCTS film showed peaks at 325 cm^{-1}, 364 cm^{-1}, and 281 cm^{-1} respectively (Fig. 2a and b). The peak at 325 cm^{-1} corresponds to the symmetric vibrational motion of S atoms in CCTS crystal structure [16, 7]. The peak at 281 cm^{-1} is attributed to the vibrations of the Co and S atoms with some contribution from the Cu atoms in the CCTS crystal structure [7, 16 - 17]. The peak at 364 cm^{-1} ascribes to the vibrations of the Sn and S atoms with some contribution from the Cu atoms in the CCTS [7, 16 -17]. The absence of the peaks at 318 cm^{-1} (orthorhombic - Cu_3SnS_4) [18], 303 cm^{-1} (cubic-

Cu_2SnS_3) and 475 cm^{-1} (hexagonal - $Cu_{2-x}S$) confirms the phase purity of synthesized nanoparticles and sulfurized films [19].

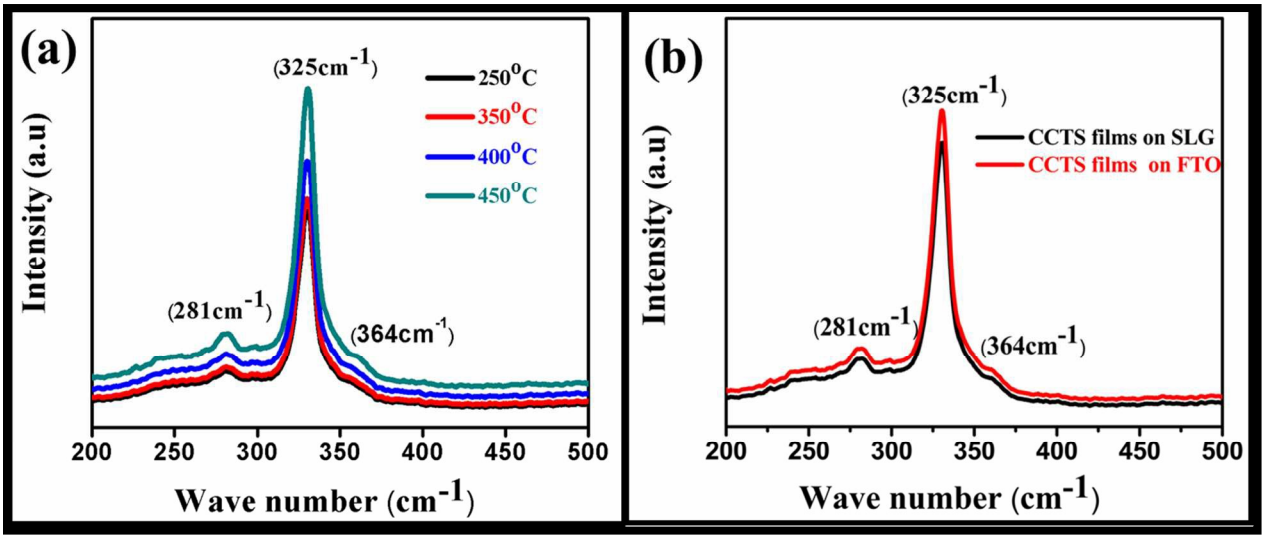

Fig. 2 Raman spectra of CCTS (a) nanoparticles synthesized at 250°C, 350°C and 450°C for 1h, (b) films sulfurized at 500°C for 30 min

Bright field TEM image of CCTS shows approximately 10 - 13 nm size spherical nanoparticles (Fig. 2a and 2b). The measured particles size, from TEM analysis, is in good accordance with the crystallite size calculated from the XRD analysis. The morphology of the nanoparticles obtained via thermal decomposition process is found to be similar to the nanoparticles previously synthesized by solvothermal and hot injection processes [8 - 9]. High-Resolution TEM (HRTEM) image of one of the individual nanoparticle shows the clear lattice fringes that indicate the crystallinity of the sample prepared at 250°C for 1 h**.** From the HRTEM, XRD and Raman analysis it is confirmed that synthesis at 250°C for 1 h is sufficient to form crystalline CCTS nanoparticles. The distance between adjacent lattice fringes is found to be 0.311 nm that corresponds with the (112) d-spacing for stannite (tetragonal) structure of CCTS (Fig. 3c). The selected area electron diffraction (SAED) taken over multiple particles show the

concentric ring patterns of CCTS (Fig. 3d). The patterns are indexed as (112), (204) and (312) planes; which corresponds to the stannite crystal structure of CCTS. EDS analysis was employed to determine the elemental composition (atomic %) of the synthesized nanoparticles at different temperatures for 1 h, and the estimated results are summarized in Table 1. Nanoparticles synthesized at 250°C have sulfur deficient and also observed chloride in the sample (Table.1). As temperature increases from 250°C to 450 °C; samples found to be slightly Sn-deficient and copper rich. The Sn-deficiency might be due to the vapourization of Sn at high temperatures [20]

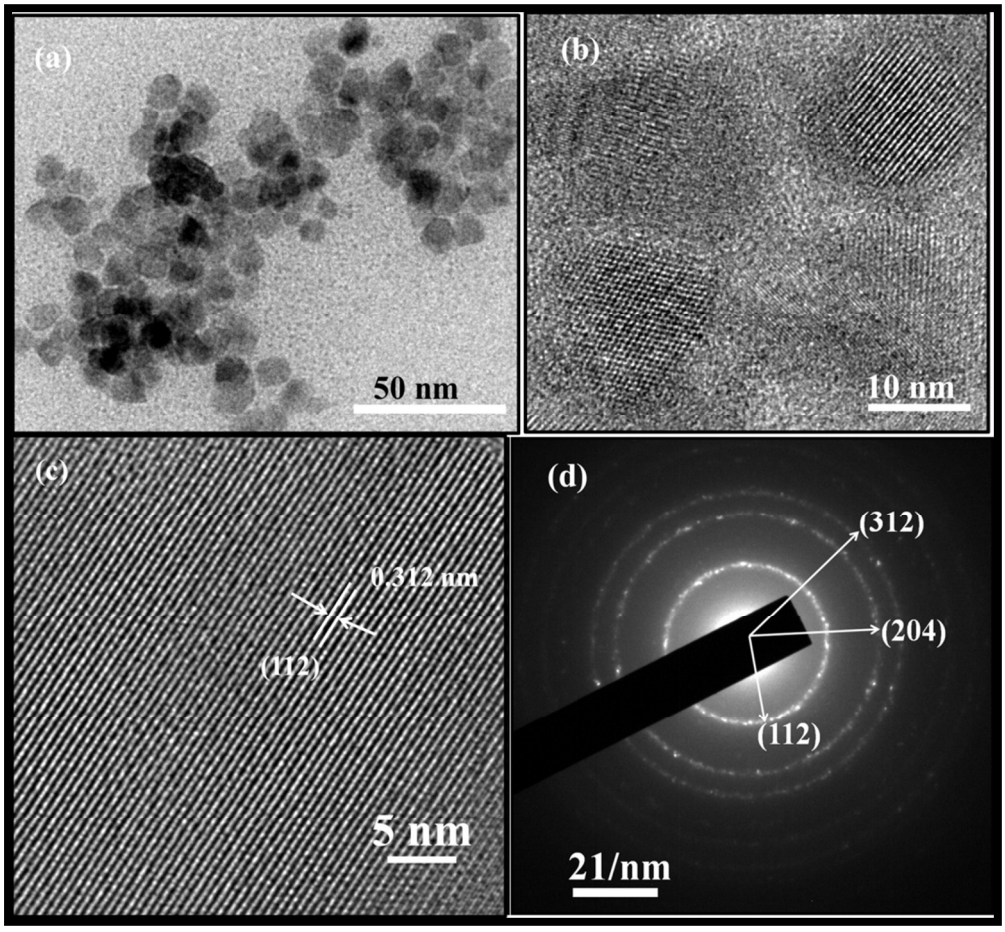

Fig. 3(a) FEG-TEM image of CCTS nanoparticles synthesized at 250°C for 1h (a) and (b) FEG-TEM, (c) HR-TEM, and (d) SAED pattern of CCTS nanoparticles

Table 1 EDS analysis of synthesized nanoparticle at different temperature for 1 h

Synthesis temperature	**250°C for 1h**	**300°C for 1h**	**350°C for 1h**	**400°C for 1h**	**450°C for 1h**
Cu (atomic %)	25	25	26	26	27
Co (atomic %)	11	12	12.5	12.5	12.5
Sn (atomic %)	12	12	11.5	11.0	10.5
S (atomic %)	47	48	50	50	50
Cl (atomic %)	5	3	-	-	-

Surface and cross-sectional FEG-SEM micrographs of the CCTS film are useful for morphology studies and thickness measurements. The surface feature reveals that grain size of CCTS film on an SLG substrate (Fig. 4a) is slightly larger than the FTO substrate (Fig. 4b). The larger grain size of the former (coated over SLG) might be due to the diffusion of sodium ions into the CCTS film [21 - 22]. Fig. 3a and 3b show a CCTS film free from cracks and pin holes. The cross-sectional micrograph of CCTS film reveals that it is dense in form and has good adherence to the SLG and FTO substrates (Fig. 4c, 3d). To further confirm the adhesion of the sulfurized CCTS films to the FTO and SLG substrate, the adhesion test was performed using ultrasonicator for 1 h. No significance changes are observed in both the films after 1 h. The ultrasonication test indicates that the films are well adherent to the FTO and SLG substrate. The thickness of the films coated on SLG and FTO substrate are found to be 400 nm and 250 nm. From EDS analysis, the average atomic weight % of elements of sulfurized CCTS film are found to be: Cu: Co: Sn: S = 25 %: 12.5 %: 10.5 %: 52 %. The obtained elemental composition ratio is found to be Cu: Co: Sn: S = 2.05: 1.00: 0.84: 4.04 respectively.

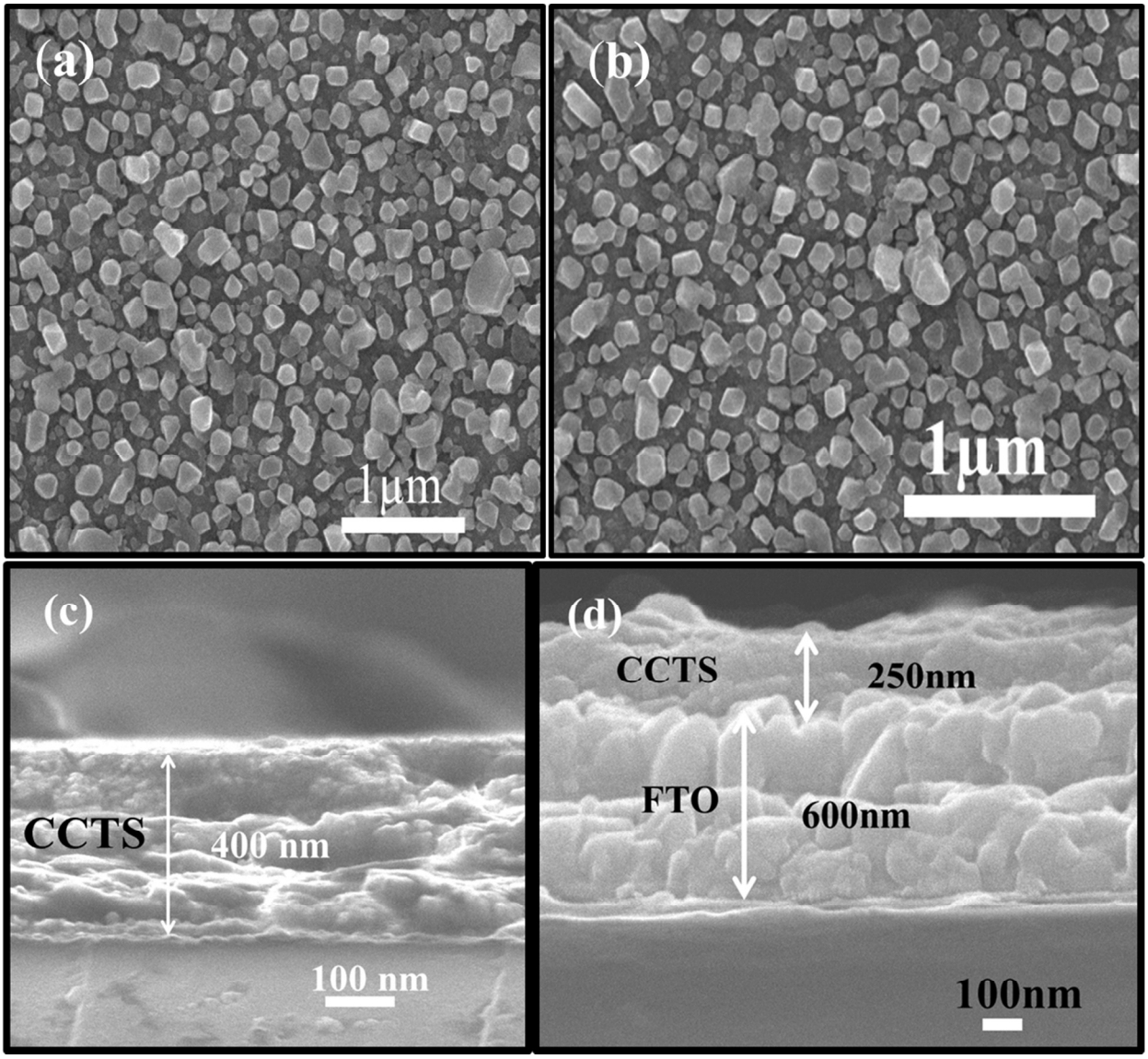

Fig. 4 FEG-SEM micrographs of (a) planner and (c) cross-sectional image of CCTS film on SLG substrate,(b) and (d) planner and a cross-sectional image of CCTS film on FTO substrate respectively.

The resistivity of the sulfurized CCTS film measured by four probe method is found to be 3.2 $x10^{-3}$ Ωm. Electrical properties of the CCTS film obtained from Hall measurements are found to be: carrier mobility = 36 cm^2/V s, carrier concentration = $2x10^{16}$ cm^{-3}, and resistivity =2 x 10^{-3} Ωm. Resistivity obtained from the Hall measurements is in good agreement with the value that is obtained by the four probe technique. The obtained electrical properties of the

CCTS film are found to be similar to the reported properties of CFTS film [23]. Hall measurements also confirm that CCTS film is a p-type semiconductor.

Mott-Schottky (MS) analysis was used to find the flat-band potential, carrier type, and carrier concentration. The MS ($1/C^2$ vs. V) plot of CCTS films in 0.1 M Na_2SO_4 is shown in Fig. 5. The negative of the slope of the MS plot confirms the p-type conductivity of the CCTS film (Fig. 5). The flat band potential (V_{FB}) is calculated by extrapolation of the linear portion X-axis of the MS plot and is found to be 0.68 V. The V_{FB} value is useful for determining the position of valence band and conduction band edges of a semiconductor at the electrode (CCTS in present study) and electrolyte interface [24].

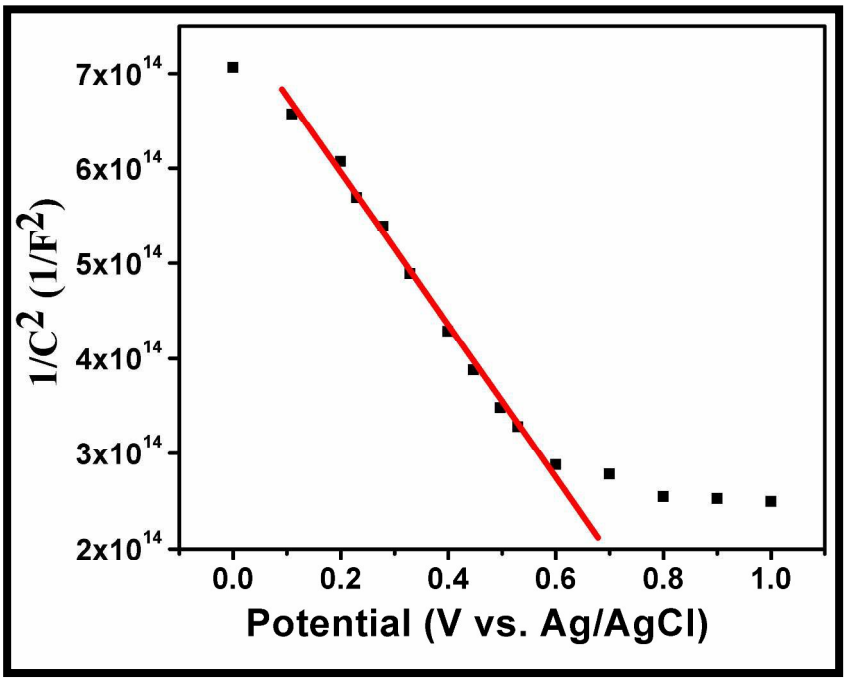

Fig. 5 Mott-Schottky ($1/C^2$ vs. V) plot for sulfurized CCTS film coated on FTO substrate

The band gap is obtained by extrapolating the linear region of the plot $(\alpha h\nu)^2$ vs. $h\nu$ and taking the intercept on the X-axis (Fig. 6 a). The optical bandgap value of CCTS film coated on SLG and FTO substrate is found to be 1.46 eV and 1.61 eV respectively. These values are in

accordance with the reported band gap values for absorber layer application [8 - 11]. The photoresponse of sulfurized CCTS films was investigated by studying the current-voltage (I-V) characteristics in dark and under illumination (Fig. 6b). According to previous studies, the photoresponse of the different absorber materials was reported at the wide range of bias voltages ranging from 500 mV to 10 V [8 - 10, 25 - 30]. In the present study, for a better understanding of the photoresponse of the absorber, the photocurrent and responsivity of the CCTS film is reported at different bias voltages. The responsivity of the CCTS is calculated by using equation 1 [25]. The photocurrent and responsivity of the CCTS film calculated from IV curves are listed in Table 2. From the Table 2, the photocurrent and responsivity of CCTS film are increasing linearly with the bias voltage.

$$\text{Responsivity } R_\lambda = (I_L - I_d)/ /P_\lambda \times A \ (AW^{-1}) \qquad 1$$

Where, R_λ is responsivity (the photocurrent generated per unit power of the incident light used on the CCTS film of the effective area (0.25 cm^2)), P_λ is the intensity of the illumination (100 mW/cm^2), A is effective area of CCTS film, I_L and I_d are current generated under illumination and dark respectively.

Table 2 Photocurrent and responsivity of the CCTS film at different bias voltages

Bias voltage	**I_L (under Illumination) (mA)**	**I_d (under dark) (mA)**	**Photo current $I_p = (I_L - I_d)$ (mA)**	**Responsivity $R_\lambda = Ip /(P_\lambda \times S)$ (AW^{-1})**
1.0	0.0740	0.0277	0.0463	0.18
2.0	0.1196	0.0629	0.0567	0.23
4.0	0.2265	0.1441	0.0824	0.32
6.0	0.3268	0.2289	0.0979	0.39
8.0	0.4448	0.3208	0.124	0.49
10.0	0.5355	0.4068	0.130	0.52

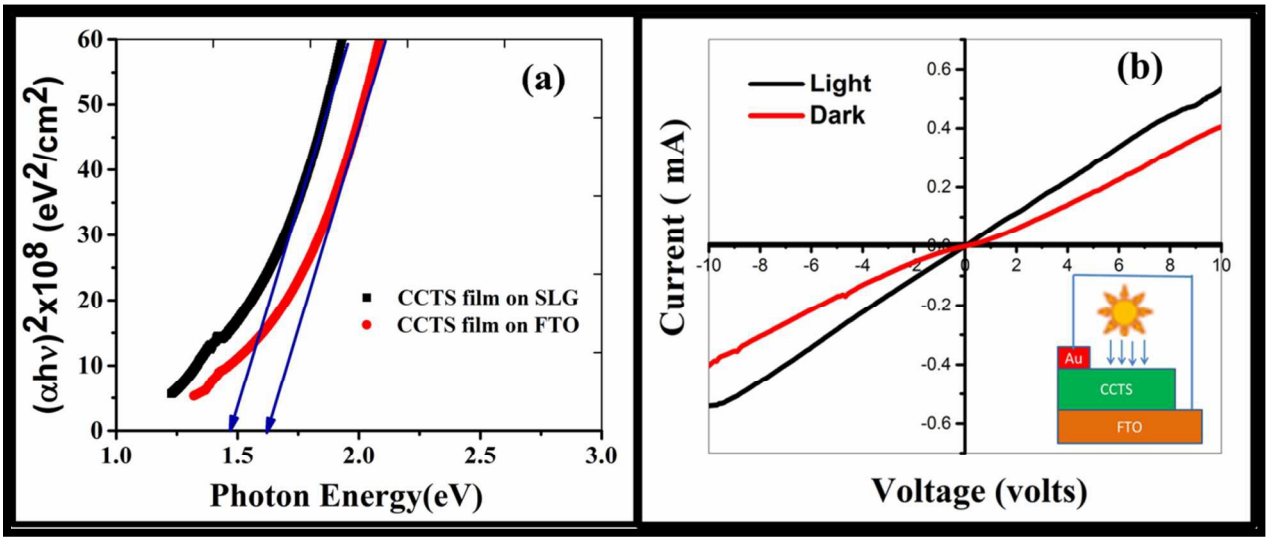

Fig. 6(a) Plot of $(\alpha h\nu)^2$ vs. hν for sulfurized CCTS film coated on FTO and SLG substrate (b) Current – voltage (I-V) curve of CCTS films coated on FTO substrate in dark and under AM 1.5 illumination (Inset Fig. 6b device structure for IV measurements).

Under illumination, an increase in the number of charge carriers in CCTS and presence of intrinsic defects in the film are responsible for the enhancement of current [8, 30]. This photo response suggests that CCTS can serve to be a potential absorber layer for the fabrication of cost-effective thin film solar cells.

4. Conclusions

In summary, earth abundant quaternary chalcopyrite, Cu_2CoSnS_4 (CCTS) nanoparticles have been synthesized successfully by thermal decomposition process at a lower temperature with shorter processing time (250^{o}C for 1 h). The nanoparticle-based ink coated was over fluorine-doped tin oxide (FTO), soda lime glass (SLG) substrate via inexpensive spin coating process to form films. XRD and Raman spectroscopy analysis confirmed the phase purity of the synthesized nanoparticles and sulfurized films. Morphology and size of synthesized nanoparticles were studied with the help of FEG-TEM analysis and is found to be spherical in

shape having a particle size of approximately 10 - 15 nm. Elemental composition of the synthesized nanoparticles and sulfurized films are found to be nearly stoichiometry ratio. These materials characteristics are similar to the CCTS nanoparticles synthesis conventional solution processes. Thus, thermal decomposition process has the potential for large-scale production at low temperature for short process time. The p – conductivity of the CCTS film has been confirmed by Mott-Schottky analysis and Hall measurements for the first time. The enhancement of photocurrent of CCTS film under illumination and the obtained optimal band gap value (1.46 - 1.61 eV) indicates its suitability as a promising absorber material for cost-effective thin film solar cells.

Acknowledgements

The authors would like to acknowledge DST, SERIIUS, NCPRE, and IITB for financial support and SAIF, IRCC for the analytical instrument facility supporting the present work.

References

[1] D. B. Mitzi, O. Gunawan, T. K. Todorov, K. Wang and S. Guha, Sol. Energy Mater. Sol. Cells, 2011, **95**, 1421 – 1436.

[2] M. A. Green, K. Emery, Y. Hishikawa, W. Warta and E. D.Dunlop, Prog. Photovolt: Res. Appl., 2015, **23**, 1 - 9.

[3] W.Wang, M. T. Winkler, O. Gunawan, T. Gokmen, T. K. Todorov, Y.Zhu, and D. B. Mitzi, Adv. Energy Mater.**,** 2014, **4**, 1301465 (1-5)

[4] Q. Guo, G. M. Ford, H. W. Hillhouse and R. Agrawal, Proceeding of 37th IEEE Photovoltaic Specialists Conference, Seattle, US, 003522, 2011.

[5] C. K. Miskin, W. C. Yang, C. J. Hages, N. J. Carter, C. S. Joglekar, E. A. Stach, and R. Agrawal, Prog. Photovolt: Res. Appl., 2015, **23**, 654 – 659

[6] T. K. Todorov, O. Gunawan and D. B. Mitzi, Prog. Photovolt: Res. Appl., 2013, **21,** 82-87.

[7] M. Benchikri, O. Zaberca, R. El Ouatib, B. Durand, F. Oftinger, A. Balocchi, J.Y. Ching, Mater let., 2012, **68**, 340 – 343

[8] X. Zhang, N. Bao, B. Lin and A. Gupta, Nanotechnology., 2013, **24**, 105706 - 8.

[9] Y. Cui, R. Deng, G. Wang and D. Pan, J. Mater. Chem., 2012, **22,** 23136 – 23140.

[10] L. Shi, Y. Li, H. Zhu, and Q. Li, Chem. Plus. Chem., 2014, **79**, 1638 – 1642

[11] B. Murali and S. B. Krupanidhi, J. Appl. Phys., 2013, **114**, 144312 - 5

[12] C. Xiao, K. Li, J. Zhang, W. Tong, Y. Liu, Z. Li, P. Huang, B. Pan, H. Su and Y. Xie, Mater. Horiz., 2014, **1**, 81 – 86

[13] M. V. Kovalenko, M. Scheele, D. V. Talapin, Science., 2009, **324,** 1417 - 1420.

[14] J. S. Lee, M. V. Kovalenko, J. Huang, D. S. Chung, D. V. Talapin, Nature Nanotechnology, 2011, **6**, 348 - 352.

[15] K. Mokurala, S. Mallick, P. Bhargava, Mater. Chem. Phys., 2014, **147**, 371 - 374.

[16] M. Himmrich, and H. Haeuseler, Specmchimica Acta., 1991, **47A**, 933 - 942.

[17] A. Khare, B. Himmetoglu, M. Johnson, D.J. Norris, M. Cococcioni, J. Appl. Phys., 2012, **111**, 083707 - 083709

[18] X. Fontané, L. C.Barrio, V. I.Roca, E. Saucedo, A. P.Rodriguez, J. R. Morante, D. M. Berg, P. J. Dale, and S. Siebentritt, Appl. Phys. Lett., 2011, **98**, 181905-3

[19] P.A. Fernandes, P.M.P. Salomé, A.F. da Cunha, J. Alloys Compd., 2011, **509,** 7600 – 7606

[20]A. Weber, R. Mainz, and H. W. Schock, J . Appl. Phys., 2010, **107**, 013516-6

[21] T. Prabhakar and N. Jampana, Sol. Energy Mater.Sol. Cells., 2011, **95**, 1001 – 1004.

[22] Q. Guo, G. M. Ford, R. Agrawal, and H. W. Hillhouse, Prog. Photovolt: Res. Appl., 2013; **21**, 64 –71

[23] R. R. Prabhakar, N. H. Loc,M. H. Kumar, P.P. Boix, S. Juan, R. A. John, S. K. Batabyal and L. H. Wong, ACS Appl. Mater. Interfaces., 2014, **6**, 17661 − 17667

[24] F. Charles, Windiest Jr., G.J. Exarhos, J. Vac. Sci. Technol., 2000, **18 A**, 1677 – 1680

[25] B. Murali, M. Madhuri, and S. B. Krupanidhi, Cryst. Growth Des. 2014, **14**, 3685−3691

[26] W. Zhang, L. Zhai, N. He, C. Zou, X. Geng, L. Cheng, Y. Dong and S. Huang, Nanoscale, 2013, **5,** 8114 – 8121

[27] L. Shi and Y.Li, RSC Adv., 2014, **4**, 43720 – 43724

[28] K. Ramasamy, X. Zhang, R. D. Bennett and A. Gupta, RSC Adv., 2013, **3**, 1186 – 1193

[29] S. R. Moulik, S. Samanta, and B. Ghosh, Appl. Phys. Lett., 2014, **104,** 232107 -4

[30] A. Kamble, K. Mokurala, A. Gupta, S. Mallick and P. Bhargava, Mater Lett., 2014, **137,** 440 - 443.